Resonance production and transverse spectra in $\bar{p}n$ annihilations at 5.55 GeV/c

H. Braun, A. Fridman,* J. -P. Gerber, P. Juillot, N. Kurtz, G. Maurer, A. Michalon, M. -E. Michalon-Mentzer, and C. Voltolini

Centre de Recherches Nucléaires and Université Louis Pasteur, Strasbourg, France

(Received 29 December 1978)

We present results on the production of resonances (ρ, f, g, ω, A_1, and A_2) in $\bar{p}n$ annihilations at 5.55 GeV/c. Channel and resonance cross sections are determined and compared with $\bar{p}p$ data obtained at nearly the same incident momentum. Production features in terms of the transverse momentum (P_T) and the transverse kinetic energy (E_K) are also investigated. In particular, it is shown that the noninvariant E_K distributions for exclusive annihilation channels can be parametrized by $e^{-E_K/T}$ functions, and the behavior of the slope parameters T is discussed.

I. INTRODUCTION

In this work we present results of $\bar{p}n$ annihilations at 5.55-GeV/c incident momentum obtained from a bubble-chamber experiment. The reactions which will be investigated are

$$\bar{p}n \rightarrow 2\pi^-\pi^+(\pi^0),$$
$$\rightarrow 3\pi^-2\pi^+(\pi^0),$$
$$\rightarrow 4\pi^-3\pi^+(\pi^0),$$
$$\rightarrow 5\pi^-4\pi^+(\pi^0).$$

We also studied channels having the same number of charged particles as above but with a neutral system containing more than one neutral particle.

The experimental procedure and the cross-section determination of the various channels will be discussed in the next section. Then we will examine (Sec. III) the production of resonances in the different final states. In Sec. IV some general aspects of the annihilation processes will be studied.

II. EVENT SELECTION AND CROSS SECTIONS

The data for this presentation have been extracted from a 150 000-picture exposure of the 30-in. deuterium-filled bubble chamber at the Argonne Zero Gradient Synchrotron. The film was scanned for even-prong events having a positive track stopping in the chamber and also for odd-prong events, (i.e., with a spectator proton below the threshold detection of the chamber). The events were processed through the standard CERN chain of programs and identified by kinematical fitting and comparison between the observed and calculated track ionization. Further cuts, essentially on the missing mass squared and the χ^2 probability, allowed us to obtain unbiased samples of fitted events. This can be seen, for instance, from the $\bar{p}n$ c.m. angular distributions of the pions which are found to be symmetric as

required by G-parity conservation.

For the so-called "missing-mass" events, i.e., those where more than one neutral particle is produced, the main selection criteria consist of choosing events where both the missing mass squared and the missing energy are positive. Figure 1 presents, for the $\bar{p}n \rightarrow 2\pi^+3\pi^-X^0$ channel thus selected, the c.m. angular distributions of the produced particles. One observes from this figure that the symmetry properties of the distribution are rather well verified. Let us note that if X^0 contains an $\bar{n}n$ pair there are no symmetry conditions for the angular distributions of
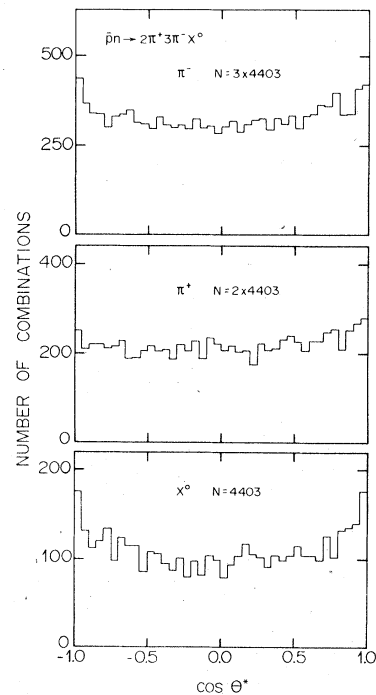
FIG. 1. The c.m. angular distributions of the $\pi^\pm$ and the X^0 systems obtained from the $\bar{p}n \rightarrow 2\pi^+3\pi^-X^0$ channels. Here X^0 is any neutral system having more than one neutral particle.
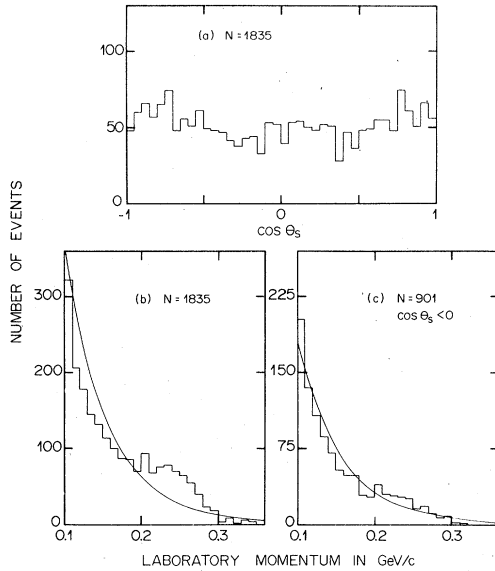
FIG. 2. The $\cos\theta_s$ distribution for all our fitted events, θ_s being the spectator proton emission angle defined in the laboratory system with respect to the beam direction (a). The laboratory momentum distribution of the spectator for all the events (b) and for those emitted backward in the laboratory system (c). The full lines represent the Hulthén-wave-function predictions.

TABLE I. Values of $\bar{p}n$ and $\bar{p}p$ annihilation cross sections at 5.55 GeV/c and 5.7 GeV/c, respectively. The $\bar{p}p$ cross sections are taken from the following: (a) H. Braun *et al.*, Nucl. Phys. B95, 481 (1975); (b) A. Accensi *et al.*, Phys. Lett. 20, 557 (1966); (c) K. Böckmann *et al.*, Nuovo Cimento 42A, 954 (1966); (d) V. Alles-Borelli *et al.*, *ibid.* 50A, 776 (1967); (e) G. Maurer, Thèse, Strasbourg, 1970 (unpublished); (f) A. Fridman *et al.*, Phys. Rev. 176, 1595 (1968). If more than one experimental result exists for a given channel, the weighted averages and errors were taken.

$\bar{p}n$ channels	Cross section (mb)	$\bar{p}p$ channels	Cross section (mb)
$\pi^+2\pi^-\pi^0$	0.43 ± 0.06	$\pi^+\pi^-\pi^0$	0.12 ± 0.01 [a]
$2\pi^+3\pi^-$	0.21 ± 0.03	$2\pi^+2\pi^-$	0.16 ± 0.02 [b,c]
$2\pi^+3\pi^-\pi^0$	1.49 ± 0.17	$2\pi^+2\pi^-\pi^0$	0.83 ± 0.07 [c,d]
$3\pi^+4\pi^-$	0.30 ± 0.05	$3\pi^+3\pi^-$	0.32 ± 0.04 [c,e]
$3\pi^+4\pi^-\pi^0$	0.77 ± 0.10	$3\pi^+3\pi^-\pi^0$	1.76 ± 0.13 [c,e]
$4\pi^+5\pi^-$	<0.03	$4\pi^+4\pi^-$	0.12 ± 0.01 [f]
$4\pi^+5\pi^-\pi^0$	0.11 ± 0.02	$4\pi^+4\pi^-\pi^0$	0.25 ± 0.02 [f]

the π's. In fact, based on the missing-mass distribution (the mass of the X^0 system) the contamination of $\bar{m}n$ among the X^0 system in the $\bar{p}n \to 2\pi^+3\pi^-X^0$ reaction is smaller than 2.6%. This assures us that in the case of Fig. 1 we are dealing practically

exclusively with annihilation events. Owing to the small statistics, the other missing-mass channels will not be studied here.

We based our cross-section calculation on the even-prong events where the stopping track was recognized as a spectator proton (p_s). To deter-
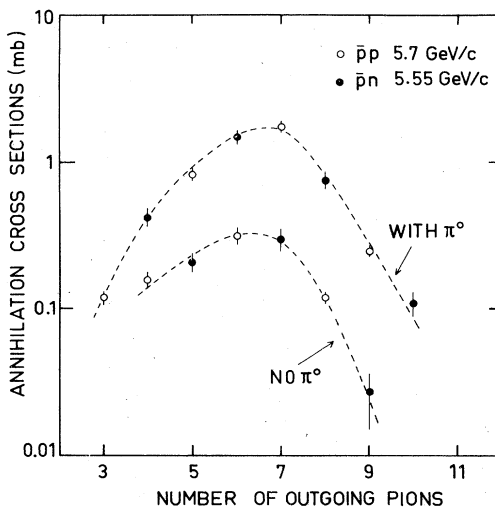
FIG. 3. Comparison of the $\bar{p}p$ and our $\bar{p}n$ cross sections as a function of the number of outgoing pions for reactions having at most one π^0 in the final state. The curves are drawn to guide the eye.
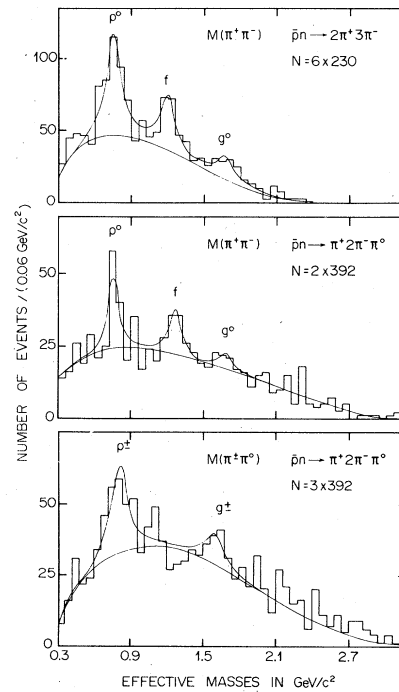
FIG. 4. Various two-pion effective-mass $[M(\pi\pi)]$ distributions obtained from the $\bar{p}n \to 2\pi^+3\pi^-$ and $\bar{p}n \to \pi^+2\pi^-\pi^0$ reactions. The data were fitted with an incoherent mixture of phase space and Breit-Wigner functions.

TABLE II. Resonance production per event and cross section for our various subchannels. The cross section is obtained by multiplying the average number of resonances per event in a given channel by the corresponding channel cross section.

Final state	Resonances per event	Cross section (mb)
$\bar{p}n \to \pi^+2\pi^-\pi^0$		0.43 ± 0.06
$\rho^0\pi^-\pi^0$	0.14 ± 0.02	0.06 ± 0.02
$f\pi^-\pi^0$	0.10 ± 0.02	0.04 ± 0.01
$g^0\pi^-\pi^0$	0.04 ± 0.01	0.02 ± 0.01
$\rho^\pm\pi^\mp\pi^-$	0.28 ± 0.04	0.12 ± 0.03
$g^\pm\pi^\mp\pi^-$	0.11 ± 0.02	0.05 ± 0.01
$\omega\pi^-$	≤0.015 ± 0.010	≤0.007 ± 0.005
$\bar{p}n \to 2\pi^+3\pi^-$		0.21 ± 0.03
$\rho^0\pi^+2\pi^-$	0.98 ± 0.07	0.21 ± 0.04
$f\pi^+2\pi^-$	0.53 ± 0.05	0.11 ± 0.03
$g^0\pi^+2\pi^-$	0.26 ± 0.03	0.05 ± 0.02
$\bar{p}n \to 2\pi^+3\pi^-\pi^0$		1.49 ± 0.17
$\rho^0\pi^+2\pi^-\pi^0$	0.28 ± 0.02	0.42 ± 0.08
$f\pi^+2\pi^-\pi^0$	0.08 ± 0.02	0.12 ± 0.04
$\rho^\pm\pi^\mp\pi^+2\pi^-$	0.12 ± 0.02	0.19 ± 0.05
$\omega\pi^+2\pi^-$	0.11 ± 0.02	0.17 ± 0.05
$A_1^\pm2\pi^-\pi^0$	0.08 ± 0.01	0.13 ± 0.03
$A_2^\pm2\pi^-\pi^0$	0.10 ± 0.01	0.16 ± 0.03
$\bar{p}n \to 3\pi^+4\pi^-$		0.30 ± 0.05
$\rho^02\pi^+3\pi^-$	1.64 ± 0.23	0.49 ± 0.15
$\bar{p}n \to 3\pi^+4\pi^-\pi^0$		0.77 ± 0.10
$\rho^02\pi^+3\pi^-\pi^0$	0.60 ± 0.12	0.46 ± 0.15
$\omega2\pi^+3\pi^-$	0.37 ± 0.05	0.29 ± 0.08
$\bar{p}n \to 4\pi^+5\pi^-$		<0.03
$\rho^03\pi^+4\pi^-$		<0.12
$\bar{p}n \to 4\pi^+5\pi^-\pi^0$		0.11 ± 0.02
$\rho^03\pi^+4\pi^-\pi^0$	0.64 ± 0.23	0.07 ± 0.04
$\omega3\pi^+4\pi^-$		<0.13

mine the various channel cross sections we used the impulse-approximation model assuming in particular that the spectator nucleon is not affected by the interaction. The number of unseen spectators is then obtained by choosing a given wave function for the deuteron taken throughout as the Hulthén wave function. This approach is certainly oversimplified as can be seen from Fig. 2(b) which presents the laboratory momentum distribution of the spectator obtained from all our fitted even-prong events. One notices an important excess of events above the Hulthén wave-function prediction for p_s momentum around 250 MeV/c. In contrast the $\cos\theta_s$ distribution [Fig. 2(a)] presents the expected isotropic behavior for the spectator.[1] Here $\cos\theta_s$ is the laboratory emission angle of the p_s defined with respect to the incident particle. By taking only events with $\cos\theta_s < 0$, namely, those for which the spectator is unambiguously identi-

fied, one obtains rather good agreement between the experimental distribution and the Hulthén prediction [Fig. 2(c)]. The observed discrepancy in the forward hemisphere ($\cos\theta_s > 0$) can be due to misidentification of spectators, to double scattering, or to final-state interactions. For the present data the misidentification of the spectator does not appear to explain the discussed effect as the numbers of forward ($\cos\theta_s > 0$) and backward ($\cos\theta_s < 0$) emitted p_s are nearly equal. Therefore, we consider these p_s spectator protons even if their momentum distribution does not agree with the Hulthén wave-function predictions in the forward hemisphere. Thus the number of unseen p_s in each channel is simply obtained by multiplying the number of p_s above 100 MeV/c by a constant factor deduced from the Hulthén wave function. Let us note that nearly the same values would be obtained if the calculation were based only on the events in the $\cos\theta_s < 0$ region.

Correcting our data for scanning losses as well as for losses due to stopping tracks too steep to be measured successfully, we obtain the $\bar{p}n$ cross sections given in Table I. These annihilation channels are also compared in Table I and in Fig. 3 with $\bar{p}p$ cross sections at nearly the same incident momentum (5.7 GeV/c). We see from this figure that the $\bar{p}p$ and $\bar{p}n$ multipion annihilation cross sections are distributed on two smooth curves characterized by the presence or the absence of a π^0 in the final state.

Some theoretical studies[2] have suggested that the π trajectory in the s channel may play an important role in $\bar{N}N$ annihilations. This implies among other things that at a given c.m. energy, states with an odd number of pions contribute dominantly to the annihilation cross sections. One may thus conjecture that for fitted annihilation reactions, states with an odd number n_0 of pions will have greater cross sections than those with $n_0 \pm 1$. Although this is really the case for $\bar{p}p$ annihilations, it is no longer true for $\bar{p}n$ annihilations. The comparison of $\bar{p}p$ and $\bar{p}n$ annihilation data (Fig. 3) clearly shows that the presence of a π^0 in the final state enhances the cross sections. As the π^0 appears in $\bar{p}p$ and $\bar{p}n$ annihilations for an odd or even number of produced pions, respectively, the alternations observed in the $\bar{p}N$ cross sections are not due to a G-parity effect. In any case the comparison of the cross sections of $\bar{p}p$ and $\bar{p}n$ annihilation channels with the same number of outgoing pions shows that the channels with a π^0 have always the largest cross sections. In fact, an intuitive explanation of this alternation effect can be obtained from multiperipheral models with a nucleon trajectory exchange. Then the positive or negative charge of the outgoing pion has to alter-
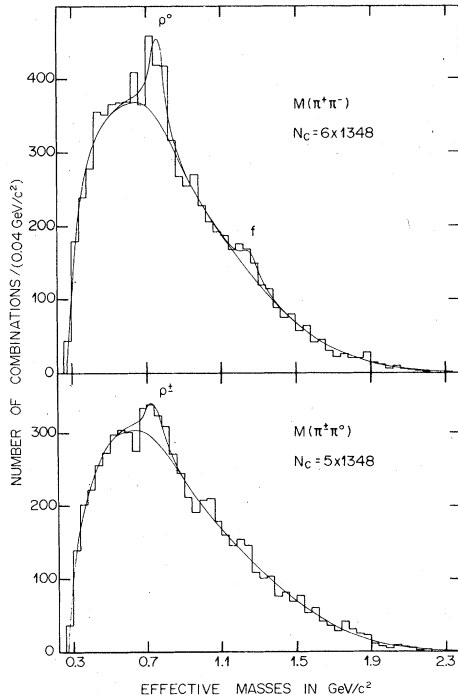
FIG. 5. The $\pi^+\pi^-$ (top) and $\pi^\pm\pi^0$ (bottom) effective-mass distributions obtained from the $\bar{p}n \to 2\pi^+3\pi^-\pi^0$ channel. The data were fitted with an incoherent mixture of phase space and Breit-Wigner functions.

nate along the multiperipheral chain. A π^0, however, can be placed anywhere in this chain. As a result of this freedom, one can then conceive that the multipion cross section tends to increase
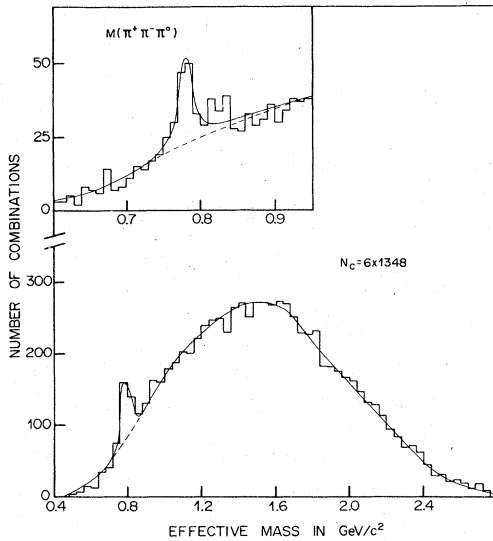
FIG. 6. The $\pi^+\pi^-\pi^0$ mass spectrum obtained from the $\bar{p}n \to 2\pi^-3\pi^+\pi^0$ reaction. The full line represents a fit to the data using an incoherent mixture of phase space and a Gaussian function for representing the ω resonance.

whenever a π^0 is present among the secondaries.[3]

One can also notice that the sums of the cross sections with π^0 for $\bar{p}p$ $[\sigma_{odd}(\bar{p}p) = 2.96 \pm 0.23$ mb$]$ and $\bar{p}n$ $[\sigma_{even}(\bar{p}n) = 2.80 \pm 0.35$ mb$]$ are nearly equal. A similar equality is also observed for reactions without a π^0 $[\sigma_{even}(\bar{p}p) = 0.51 \pm 0.11$ mb and $\sigma_{odd}(\bar{p}n) = 0.60 \pm 0.07$ mb$]$.

III. RESONANCE PRODUCTION

The studied channels present a rather copious resonance production. Even in the channels with limited statistics, as for instance the $\bar{p}n \to \pi^+2\pi^-\pi^0$ (392 events) and $\bar{p}n \to 2\pi^+3\pi^-$ (230 events) reactions, one clearly sees from the 2π effective-mass distributions the production of ρ, f, and g (Fig. 4). Fitting these distributions with an incoherent mixture of phase space and Breit-Wigner functions we ob-
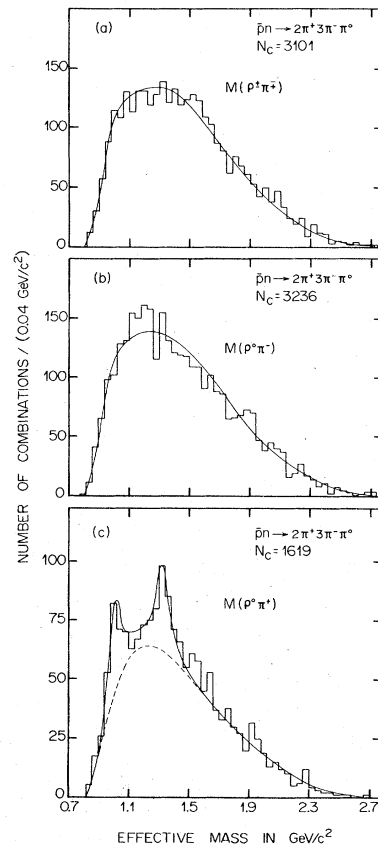
FIG. 7. The (a) $\rho^\pm\pi^\mp$, (b) $\rho^0\pi^-$, (c) $\rho^0\pi^+$ effective-mass distributions. Here the ρ is defined as a 2π mass combination in the 0.66–0.84 GeV/c^2 interval. The full lines in (a) and (b) represent the phase-space prediction normalized to the total number (N_C) of combinations. In (c) the full line is obtained by fitting the data with an incoherent mixture of phase space and two Breit-Wigner functions due to the A_1 and A_2 resonances.
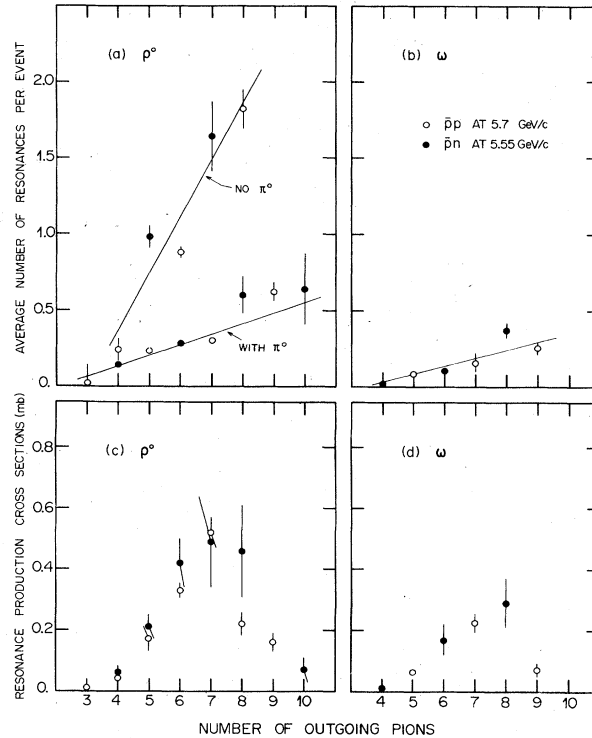
FIG. 8. The average number of ρ^0 and ω production [(a) and (b)] as a function of the number of outgoing pions for $\bar{p}n$ and $\bar{p}p$ data, with their corresponding cross sections [(c) and (d)]. The lines are drawn to guide the eye.

tain the number of resonances produced per event as given in Table II. But owing to poor statistics, we are not able to do multidimensional fits. We also give in this table the corresponding cross sections obtained simply by multiplying the average number of resonances per event in a given channel by the channel cross section. For events with high combinatorial background, as several resonances of the same type may be produced in a given event, these values are to be considered as upper limits of the inclusive resonance production cross sections for a given channel. The cross sections given in Table II are not corrected for unseen decay modes.

The most striking effective-mass distributions obtained from the $\bar{p}n \rightarrow 2\pi^+ 3\pi^- \pi^0$ (1348 events) channel are presented in Figs. 5 through 7. One notices the rather important ρ^0, $\rho^\pm$, f, and ω production. Selecting events in the ρ band, namely, those having the two-pion effective mass in the 0.66–0.84 GeV/c^2 mass range, we present in Fig. 7 the $\rho\pi$ effective-mass distributions. One observes in this figure an enhancement in the $\rho^0\pi^+$ mass in the A_1 and A_2 region while no signal is observed in the $\rho^0\pi^-$ and $\rho^\pm\pi^\mp$ distributions. The full line in Fig. 7(c) represents our best fit obtained by fixing the central values $(M_{1,2})$ and widths $(\Gamma_{1,2})$ of the A_1 and A_2 enhancement to $M_1 = 1.00$

GeV/c^2, $\Gamma_1 = 0.1$ GeV/c^2, and $M_2 = 1.32$ GeV/c^2, $\Gamma_2 = 0.1$ GeV/c^2, respectively. and using a modified phase space. This phase space has been obtained by a Monte Carlo method in which the same cuts as for the experimental data have been applied. The full lines in Figs. 7(a) and 7(b) represent the prediction of this deformed phase space. Although the fitted curve does not give a very good description of the data around the 1.1 GeV/c^2 region, the existence of the A_1 enhancement is clearly seen in Fig. 7. The fact that such an enhancement was also seen in $\bar{p}p$ annihilations at 5.7 GeV/c (see Ref. 4) supports the idea that the A_1 is a real resonance. In any case there is no Deck mechanism in annihilation processes such as that often used to explain the A_1 effect or at least a part of it in production reactions. The fact that no $A_{1,2}$ signals are seen in the $\rho^0\pi^-$ and $\rho^\pm\pi^\mp$ effective-mass distributions is surprising but it may be explained by the higher combinatorial background obtained for these systems. Furthermore, the $\rho^0\pi^+$ mass spectrum is very favorable for detecting the $A_{1,2}$ enhancement as no ρ^0 can be present in the system recoiling $(2\pi^-\pi^0)$ against the $\rho^0\pi^+$ object.

For the other annihilation channels we also have calculated the amount of resonance production as well as the corresponding cross sections. They are all summarized in Table II. In Fig. 8 we
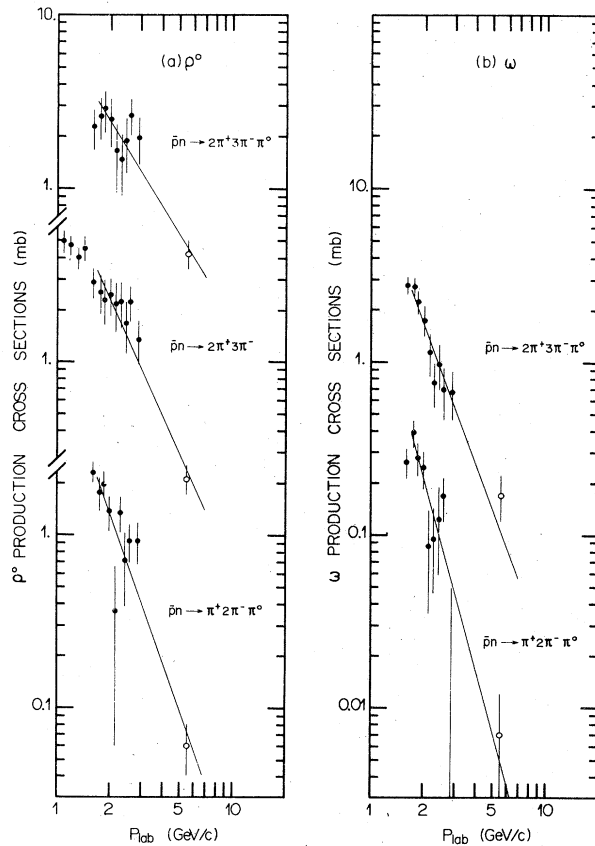
FIG. 9. Compilation of the ρ^0 and ω production cross sections for various $\bar{p}n$ channels as a function of the incident laboratory momentum (P_{lab}). The data below 3 GeV/c (dark points) are obtained from the study made by Z. Ming Ma *et al.*, Nucl. Phys. B51, 77 (1973). The lines represent power-law decreasing functions in P_{lab}.

present the average number of ρ^0 and ω production as a function of the number of outgoing pions. These production rates are compared in the same figure with $\bar{p}p$ data at 5.7 GeV/c. One notices that for a given number of outgoing pions the average number of ρ^0 production is always greater in channels without π^0. In terms of cross sections the ρ^0 and ω production in both $\bar{p}n$ and $\bar{p}p$ interactions are distributed on smooth curves [Fig. 8(c) and 8(d)]. Finally we also present a compilation of the ρ^0 and ω cross-section production in various $\bar{p}n$ channels as a function of P_{lab}, the incident $\bar{p}$ momentum (Fig. 9). Although the errors

TABLE III. The m values obtained by fitting the ρ^0 and ω cross sections as function of P_{lab}, the incident momentum, with P_{lab}^{-m} functions.

	m for ρ^0	m for ω
$\bar{p}n \rightarrow \pi^+2\pi^-\pi^0$	2.9 ± 0.2	$\geqslant 3.7 \pm 0.7$
$\bar{p}n \rightarrow 2\pi^+3\pi^-$	2.3 ± 0.2	
$\bar{p}n \rightarrow 2\pi^+3\pi^-\pi^0$	1.6 ± 0.2	2.7 ± 0.4
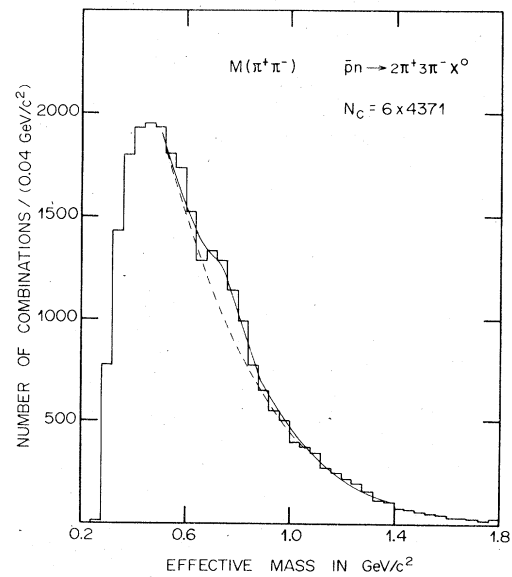
FIG. 10. The $\pi^+\pi^-$ effective-mass distribution in the missing-mass $\bar{p}n \rightarrow 2\pi^+3\pi^-X^0$ channel. The full line is obtained by fitting the spectrum with polynomial background (dashed curve under the ρ^0 bump) and a Breit-Wigner function.
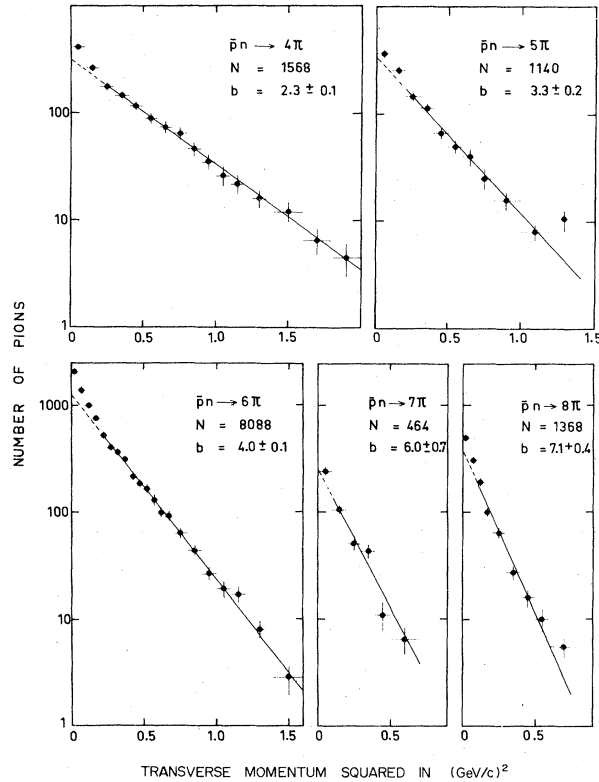
FIG. 11. The distributions of the transverse momentum squared (P_T^2) of the outgoing pions in various $\bar{p}n$ annihilation channels. The full lines represent an exponential $e^{-bP_T^2}$ fit to the data. The fitted b slopes [in $(\mathrm{GeV}/c)^{-2}$] are given in the figure (see also Table IV).

are rather important, one notices that the data tend to decrease according a P_{1ab}^{-m} power law, the fitted m values for $P_{1ab} > 1.7$ GeV/c being given in Table III.

The marked feature of the $\bar{p}n \to 2\pi^+3\pi^-X^0$ missing-mass channel consists of an important ρ^0 production. Figure 10 presents the $\pi^+\pi^-$ effective-mass distribution which was fitted with a polynomial

background and a Breit-Wigner function for the ρ^0 resonance. One thus obtains an average ρ^0 production rate of 0.25 ± 0.04.

IV. PRODUCTION FEATURES

Some aspects of production features in $\bar{p}n$ annihilations at 5.55 GeV/c have already been investi-

TABLE IV. The average of the transverse energy $E_T = (P_T^2 + m_\pi^2)^{1/2}$ for the outgoing pions and for the ρ and ω (first three rows). Values of the parameter b and T obtained by fitting the experimental P_T^2 and E_T^2 distributions with $\exp(-bP_T^2)$ and $\exp(-E_K/T)$ functions, respectively. The P_T^2 range used for the fit is indicated in Fig. 11 while T is calculated from all the data and from the π emitted in the central rapidity region (c.m. rapidity of the pions $|y^*| \leq 0.3$).

		4π	5π	6π	7π	8π
$\langle E_T \rangle$ (GeV)	π	0.58 ± 0.01	0.49 ± 0.01	0.43 ± 0.01	0.37 ± 0.01	0.35 ± 0.01
	ρ^0	1.06 ± 0.02	0.99 ± 0.01	0.44 ± 0.01	0.88 ± 0.01	0.87 ± 0.01
	ω	1.2 ± 0.2		1.01 ± 0.01		0.95 ± 0.01
b [$(\mathrm{GeV}/c)^{-2}$]	π	2.3 ± 0.1	3.3 ± 0.2	4.0 ± 0.1	6.0 ± 0.7	7.1 ± 0.4
	ρ^0	1.6 ± 0.2	2.4 ± 0.2	2.8 ± 0.1	4.4 ± 0.4	4.6 ± 0.3
	ω			2.2 ± 0.2		3.8 ± 0.3
T (MeV)	π^a	418 ± 42	265 ± 24	236 ± 5	254 ± 38	172 ± 9
	π^b	207 ± 6	176 ± 4	145 ± 2	124 ± 5	106 ± 2

$^a |y^*| \leq 0.3$. ^{b}All pions.
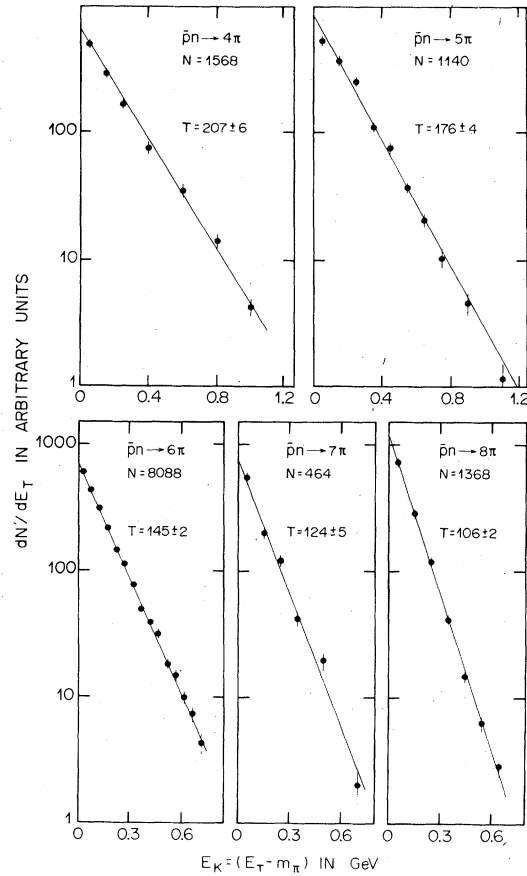
FIG. 12. The noninvariant dN'/dE_T as a function of E_K, the transverse kinetic energy. The full lines represent exponential $e^{-E_K/T}$ fits to the data. The fitted slope parameters (in MeV/c) are given in the figure.

gated. In particular, a study of the correlation between the averages of the transverse and c.m. longitudinal momenta has been carried out[5] as well as an impact-parameter analysis of annihilation reactions.[6] Here we will merely examine the transverse momentum P_T and the transverse energy $E_T = (P_T^2 + m_\pi^2)^{1/2}$ (m_π being the pion mass) behavior of the produced particles and resonances. For all the studied channels the P_T^2 distributions of the outgoing pions have an exponential $e^{-bP_T^2}$ behavior for $P_T^2 \gtrsim 0.2$ $(GeV/c)^2$ (see Fig. 11). The small accumulation of events for small P_T^2 has been observed in many production reactions and is accounted for by resonance production.[7] In contrast the P_T^2 distributions of the produced resonances present a single exponential behavior. All the fitted slopes are given in Table IV. One notices that all the slopes are increasing with n, the number of outgoing pions.

A thermodynamical approach to the understanding of the production mechanism has been used already in inclusive studies.[8] In this framework the noninvariant transverse kinetic energy E_K (here

$E_K = E_T - m_\pi$) distribution can be represented by $e^{-E_K/T}$ functions where T has a meaning of temperature. Since we do not have the fully inclusive annihilation data, we will examine the transverse kinetic energy for all of our exclusive reactions. To this end we consider the noninvariant single-particle distribution written in the form

$$\frac{d^3N}{d^3p} = \frac{1}{2\pi E^* E_T} \frac{d^2N}{dE_T dy^*} ,$$

p being the c.m. momentum of the observed particle while E^* and y^* are their c.m. energy and rapidity, respectively. The noninvariant E_T distribution $(dN'/dE_T \equiv dN'/dE_K)$ can thus be obtained from the E_T distribution in which each individual event has been weighted by $(E^* E_T)^{-1}$. These dN'/dE_T distributions are represented in Fig. 12 and are well described by $e^{-E_K/T}$ functions. Table IV gives the fitted T values as well as the average $\langle E_T \rangle$ for all the studied channels. One sees from this table that the T slopes appear to decrease with increasing of n.

Recently it has been suggested that one can re-
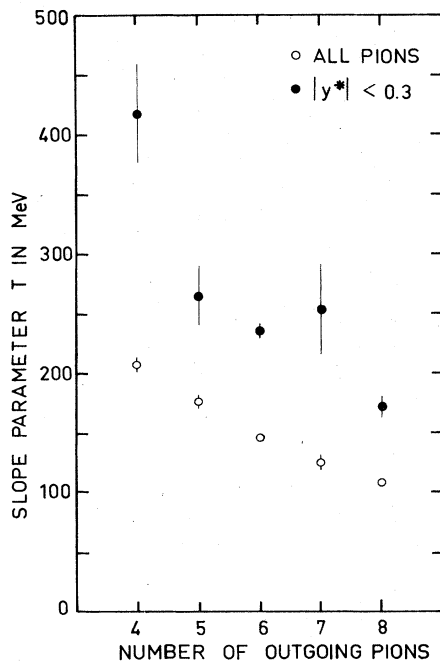
FIG. 13. The slope parameters T obtained by fitting the noninvariant transverse kinetic energy of the outgoing pions (E_K) with $e^{-E_K/T}$ functions for various annihilation channels.

late the inclusive E_K distributions in the central region with the relative transverse acceleration through the temperature concept.[9] We therefore examine the noninvariant E_K distributions of the emitted π in the central region defined by $|y^*| \leq 0.3$, y^* being the c.m. rapidity of the outgoing pions (note that now $E^* \simeq E_T$). We still observe the $e^{-E_K/T}$ behavior for the pions, but this time the temperatures T are higher than those found previously (see Table IV and also Fig. 13). Let us also note that the T found in the central region for annihilation reactions are higher than $T \sim 130$ MeV, which is the value predicted for usual inclusive production reactions.[8] This can be intuitively understood from the model of Ref. 9 as the temperature there is proportional to the inverse of the average impact parameter. Since for annihilation reactions the average impact parameter is smaller than for other production reactions,[6,10] one indeed expects $T > 130$ MeV.

To summarize we find that the distributions present a simple $e^{-E_K/T}$ behavior. This simple parametrization, which has been seen for a great variety of inclusive reactions, is thus also valid for exclusive annihilation reactions. A comparison of inclusive and exclusive annihilation reactions with other processes will certainly be useful in order to have a better understanding of the temperature concept.

---

*Now at CEN, Saclay, France.

[1]As is well known the flux factor tends to increase the $\cos\theta_s$ distribution in the $\cos\theta_s \sim 1$ region. This effect, however, can be compensated by the decrease of the cross section in the c.m. energy range introduced by the neutron Fermi motion. See for instance A. Fridman, Fortschr. Phys. 23, 243 (1975).

[2]H. Rubinstein, in Proceedings of the Symposium on Antinucleon-Nucleon Interactions, Liblice-Prague, 1974, edited by L. Montanet (CERN, Geneva, 1974).

[3]H. Braun et al., Phys. Rev. D 8, 2034 (1973).

[4]A. Fridman et al., Phys. Rev. 167, 1268 (1968).

[5]H. Braun et al., in Antinucleon-Nucleon Interactions,

proceedings of the Stockholm Symposium, 1976, edited by G. Ekspong and S. Nilsson (Pergamon, New York, 1977), p. 337.

[6]H. Braun et al., Phys. Rev. D 15, 1293 (1977).

[7]H. Kirk et al., Nucl. Phys. B128, 397 (1977).

[8]M. Deutschmann et al., Nucl. Phys. B70, 189 (1974).

[9]S. Barshay and W. Troost, Phys. Lett. 73B, 437 (1978).

[10]A. Fridman, in Proceedings of the VIII International Symposium on Multiparticle Dynamics, Kayserberg, 1977, edited by R. Arnold et al. (Centre de Recherches Nucleaires, Strasbourg, France, 1977), p. A129.